Journal of Physics D: Applied Physics

PAPER • **OPEN ACCESS**

Characterization of nitrogen thermal plasma torch: electric and gas pressure effects

To cite this article: Parham Firoozi *et al* 2025 *J. Phys. D: Appl. Phys.* **58** 345501

OPEN ACCESS
IOP Publishing
Journal of Physics D: Applied Physics
J. Phys. D: Appl. Phys. **58** (2025) 345501 (16pp) https://doi.org/10.1088/1361-6463/adfae5

Characterization of nitrogen thermal plasma torch: electric and gas pressure effects

Parham Firoozi[1], Mohammad Reza Khani[1], Farzaneh Ostovarpour[1], Babak Shokri[1,2], Abel Rouboa[3,4] and Eliseu Monteiro[3,*]

[1] Shahid Beheshti University, Laser and Plasma Research Institute, 1983963113 Tehran, Iran
[2] Department of Physics, Shahid Beheshti University, 1983963113 Tehran, Iran
[3] LAETA, Faculty of Engineering, University of Porto, Rua Dr Roberto Frias, 4200-465 Porto, Portugal
[4] Mechanical Engineering and Applied Mechanics of SEAS, University of Pennsylvania, Philadelphia, PA 19104-6391, United States of America

E-mail: emonteiro@fe.up.pt

Received 28 March 2025, revised 9 July 2025
Accepted for publication 13 August 2025
Published 26 August 2025

Abstract

The industrial applications of thermal plasma technology, particularly in material processing, have attracted considerable attention worldwide. Plasma torch is a tool that has proven its efficacy for industrial use by thermal arc plasma production. In this study, after designing and manufacturing a non-transferred type of DC plasma torch, its electrical, chemical, and thermodynamic characteristics were investigated with nitrogen working gas and variable parameters of electric current and nitrogen gas inlet pressure. The study's novelty arises from the design of a torch for plasma pyrolysis of liquid carbon-based materials, which requires that they must be sprayed into its flame from a specific angle. This study investigated and diagnosed electrical, thermodynamic, and chemical features such as voltage, voltage variations, frequency, type of voltage behavior, thermal efficiency, enthalpy, chemical and atomic species produced in plasma, as well as their excitation and rotational temperature. Results show that the flame's maximum temperature of 3492 K is achievable at 100 A current and 0.5 bar nitrogen gas inlet pressure with an enthalpy of 44.41 MJ kg^{-1} and thermal efficiency of 75.1% at 20 mm from the nozzle outlet. Comprehensiveness in examining the electrical, thermodynamic, and chemical parameters involved in the constructed plasma torch is another innovation in this study, which sheds light on how to optimize this torch to achieve high-quality results from industrial and experimental points of view.

Keywords: plasma torch, materials processing, enthalpy, thermal efficiency, restrike mode, liquid carbon-based materials

* Author to whom any correspondence should be addressed.

1. Introduction

Thermal plasma technology has a wide range of industrial and experimental applications in materials processing [1, 2], including surface coating of metals and nonmetals [3–5], material synthesis and nanoparticle manufacturing [6], production of high-quality powder from refractory materials [7], cutting and welding [8], and hazardous waste disposal [9–14]. Thermal plasma torches are acknowledged as one of the systems capable of producing thermal plasma jets powered by direct current (DC), alternating current (AC), radio frequency sources, and other electric discharge types [15–17]. Among the most common methods for thermal plasma production in industries are DC thermal plasma torches, categorized into two main groups depending on the output jet velocity and power of the created plasma. The first group is characterized by a higher output velocity of the plasma jet than the second group. For this reason, while the former is best suited for coating and cutting purposes, the latter is mainly used for applications in metallurgy and waste disposal [18]. Depending on whether the waste is solid or liquid and how the waste is added to the plasma during waste disposal, the width and outlet velocity of the formed plasma jet should be wide and low, respectively. The temperature and chemical composition of the formed plasma significantly affect the decomposition rate and quality of the output product resulting from the gasification process [19]. A variety of research studies have been conducted on the manufacture of plasma torches to dispose of all industrial waste types directly, such as the disposal of urban (either solid or liquid), hospital, industrial, and radioactive wastes through the gasification and plasma pyrolysis processes or potential risk reduction of the remaining ash.

Using a thermal plasma torch, Kim *et al* [20] investigated waste disposal systems that contain polychlorinated biphenyl waste. They compared the effects of the plasma formed by air and water vapor as the working gases. Nishikawa *et al* [21] studied the designing, manufacturing, and characterizing of a DC plasma torch with water vapor and air as the working gases. In addition, they examined the effect of changing plasma torch working gas on the decomposition rate of carbon chains in the pyrolysis and gasification processes. Ni *et al* [22] studied the structure of high-power plasma torches, called Plasmatron, and their characteristics, mainly used for metallurgical applications in cement kilns and waste disposal. Nishikawa *et al* [21] designed and characterized a DC plasma torch with water vapor as the working gas under atmospheric pressure for material processing applications and the gasification of carbon material. Four years later, Cao *et al* [23] put considerable effort into designing and constructing a plasma torch with a slow plasma jet flow in the outlet area of the torch nozzle. Obraztsov *et al* [24] proposed the design, construction, and characterization of AC thermal plasma torches, which were used to process organic materials. Chau *et al* [25] conducted a numerical study and experimental characterization of DC plasma torches with water vapor as the working gas and tubular electrodes.

The present study focuses on the design and construction of thermal plasma torches, as well as their applications in carbon-based waste disposal. The novelty lies in the design of a torch for the plasma pyrolysis of liquid carbon-based materials, such as waste oils, glycerol, and bio-oils. These materials require a high-temperature, oxygen-free environment and must be sprayed into the plasma torch's flame from a specific angle. Given the assumption that the carbon material's injection distance from the torch outlet nozzle should be 20 mm, this distance was regarded the effective distance for determining which metrics are important in plasma torch characterization. The features studied include an appropriate flame width, a bulk plasma temperature of more than 3000 K, a high enthalpy of the plasma flame at the torch output, the torch's thermal efficiency, and active atomic species in the plasma flame. This study further evaluated the plasma torch's thermodynamic, chemical, and electrical characteristics, which are noteworthy in the liquid-based waste disposal system. The main designed components of the plasma torch include the nozzles, electrodes, electrical insulators, and cooling channels that distinguish this research from previous investigations regarding the assumed details.

The designed plasma torch to conduct this experimental study is a DC non-transferred cold water-cooled torch with nitrogen as the working gas. The torch geometry was specifically tailored to enable the injection of liquid materials into the core of the plasma plume at an optimized angle. This feature ensures efficient atomization and interaction of the liquid with the plasma flame, which is critical for promoting complete vaporization and molecular dissociation. The function of the plasma torch was investigated in two experimental groups. First, the plasma torch was placed at a constant working gas inlet pressure with changes in the electric current and then in a condition with a constant electric current at varying gas inlet pressures. The effect of these two variables, working gas inlet pressure and electric current, on the electrical, thermodynamic, and chemical characteristics was comparatively evaluated. Noteworthy to say that the characteristics included in the torch components' design directly affect the electrical, thermodynamic, and chemical characteristics of the species formed in the plasma. Electrical characteristics include the electric voltage, dominant frequency and behavior mode of the electric arc, and input power of the torch. The thermodynamic and chemical characteristics include thermal efficiency, plasma enthalpy, heat loss, plasma flame temperature, excitation and rotational temperatures, and atomic and molecular species present in the generated plasma arc [22, 26–30]. Among the other innovations of this research is the comprehensiveness in examining the electrical, thermodynamic, and chemical parameters involved in the constructed plasma torch.

2. Plasma torch characteristics

The structure and components of plasma torches significantly impact their function and characteristics. It should be

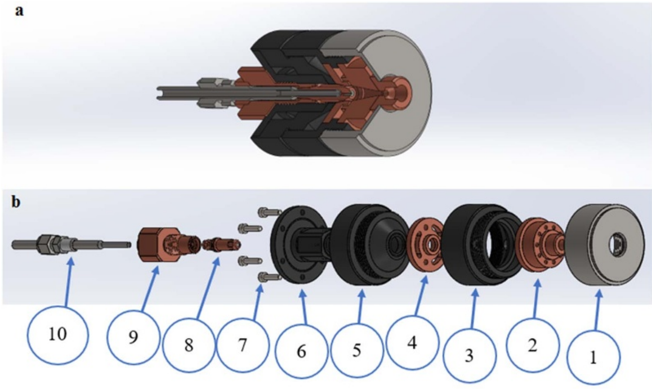

Figure 1. (a) assembled plasma torch and (b) components of the designed plasma torch.

noted that all components should be thoroughly examined in designing a torch for a specific application. DC thermal plasma torches are composed of different parts, including the exit nozzle (anode electrode), cathode electrode, a gas injection/swirl ring that makes the vortex gas flow, and the electrode's cooling system. The design of the electrodes (anode and cathode) and selection of appropriate electrode material, considering the working temperature of the torch, play a determining role in the stability of the plasma as well as the service life, corrosion of the electrode, and shape of the plasma jet [17, 26, 31–34]. The proper design of the swirl ring significantly contributes to electric arc column stabilization, heat transfer between the plasma and nozzle wall, the shape of the output plasma jet, and also cooling of the electrodes [31–33]. Further, the cooling mechanism designed for electrodes plays an essential role in determining the thermal efficiency, energy loss from the torch, and service life of electrodes [18, 32–34].

Figure 1 depicts the overall structure and components of the designed plasma torch, with numbers 1–10 corresponding to the nozzle retaining cap, nozzle (anode electrode), ignition ring holder, ignition ring, swirl ring holder, swirl ring, retaining screws, cathode electrode, cathode electrode holder, and cathode electrode cooling channel, respectively.

The swirl ring injects gas flow into the plasma formation area as it enters the torch. As a result, the vortex gas flow causes the initial ignition in the high voltage range of 7–10 kV and frequency range of 2–5 MHz. Therefore, the charge density of the electrons in this area increased, leading to the electric arc formation between the cathode electrode and anode, hence plasma jet formation at the plasma torch outlet. This torch used a converging and double-stepped nozzle made of copper. The outlet diameter and length of the nozzle were 8 mm and 30 mm, respectively. The used cathode electrode, which is 8.5 mm in diameter, is made of tungsten with copper sheathing that belongs to the button-type cathode. The gas flow inside the torch is created by a swirl ring that contains ten holes, each 1 mm in diameter.

3. Experimental setup

The necessary equipment for setting up the manufactured plasma torch and the equipment used to characterize the tested plasma torch are described in this section. The experimental setup is illustrated in figure 2.

A 30 kW transformer DC power supply to light the plasma torch is used. The power supply can maintain the current range of 20–150 A. The voltage of 10 kV and frequency of 2 MHz were applied to start the electric arc. A water pump with a pressure of 6 bar, connected to a water tank at 25 °C, was then used to cool the electrodes. Nitrogen was used as the working gas to start the plasma torch, stored in a cylinder under a pressure of 40 bar. The amount of gas entering the plasma torch was measured before entering the plasma torch using a barometer, and the temperature of the cooling water of the plasma torch at the torch inlet and outlet was also determined using two thermometers. To study the voltage and current passing through the plasma torch, a Tektronix TDS2000 oscilloscope was utilized, which was connected to a computer for data transfer. In addition, the AvaSpec-3648 device was used to estimate the chemical species in the plasma as well as the mean temperature of the plasma. In this method, the spectroscopy of the light emitted from the plasma bulk was considered to estimate the plasma's chemical species and mean temperature. It should be noted that the spectroscopic probe is located 20 mm from the nozzle outlet.

4. Results and discussion

In these experiments, the mean voltage, frequency, fluctuations, and type of electric arc behavior were determined. Then, the thermal efficiency of the torch, power dissipation, and enthalpy of the formed nitrogen plasma were evaluated. In the third stage of the tests, the molecular and atomic species formed in the plasma, the rotational temperature of the molecules, the excitation temperature, and the plasma temperature were estimated and examined. During the tests,

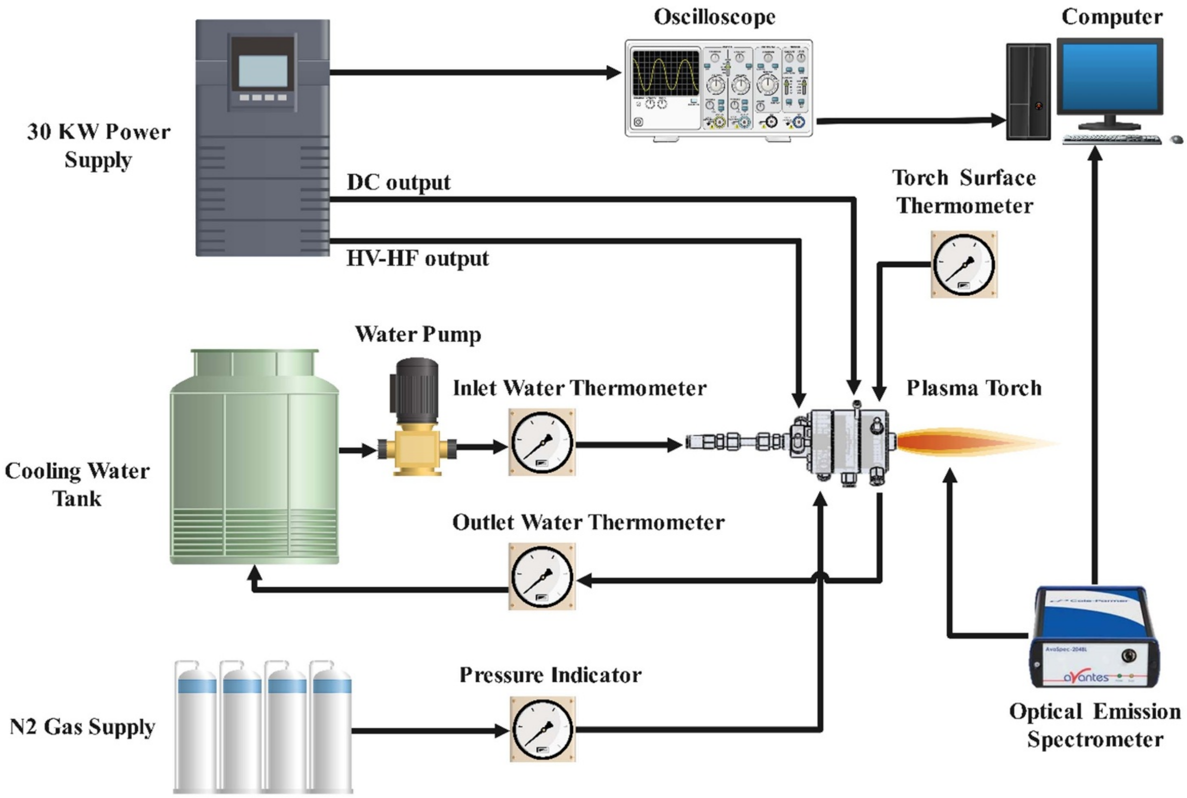

Figure 2. A view of the setup of the components designed for the plasma torch test.

investigations were carried out under two conditions: increasing the electric current at the constant working gas inlet pressure of 0.5 bar (the first condition) and increasing the working gas inlet pressure at the constant electric current of 100 A (the second condition). Finally, the obtained results were compared with each other.

4.1. Voltage versus current and gas inlet pressure

Figure 3 shows the diagrams of voltage fluctuations versus the electric current and voltage changes versus the nitrogen inlet pressure.

In figure 3(a), the nitrogen inlet pressure is a constant value equal to 0.5 bar, while the plasma torch current increased from 50 to 100 A. Consequently, the charge density in the electric arc column increased, and the electric arc became thicker, decreasing the potential difference of the torch. In figure 3(b), the electric current value of the plasma torch was set constant at 100 A, and the nitrogen pressure entering the plasma torch was elevated from 0.75 to 2.5 bar. As a result, the velocity of the plasma fluid inside the torch, the length of the electric arc, and the electric potential difference increased. In other words, with an increase in the electric current at a constant gas inlet pressure, the electric potential difference decreases, while with an increase in the nitrogen gas inlet pressure in the torch at a constant electric current, the electric potential difference increases. In this regard, it can be generally concluded that the maximum voltage of the plasma torch designed and made through electrical characterization at the nitrogen inlet pressure of 2.5 bar and electric current of 100 A is 220 V, while its minimum voltage value is 112 V at the nitrogen pressure of 0.5 bar and electric current of 50 A.

4.2. Characteristics of the voltage, frequency, and type of voltage

Voltage fluctuations and the dominant frequency of the torch voltage under different conditions are other critical electrical features of plasma torches. The number of voltage fluctuations indicates the electric arc's stability at the arc-anode attachment point. Moving electric arcs exhibit three types of behavior, namely the steady mode, in which the ratio of the voltage fluctuations to the mean voltage is less than 20%; takeover mode, in which this ratio is between 20 and 50%; and in restrike mode that is between 40 and 100%. It should be noted that the type of plasma gas can considerably affect the voltage fluctuation behavior [18, 35]. The fast Fourier transform (FFT) function derived from the voltage-time graph measured by an oscilloscope was used to estimate the dominant frequency of the electric arc movement on the anode.

The diagram of the plasma torch voltage fluctuations at different currents ranging from 50 to 100 A and nitrogen gas inlet pressure of 0.5 bar is illustrated on the left side of figure 4 in blue. The sampling time of the plasma torch voltage is 0.02 s. As observed in this figure, with an increase in the electric arc current, the mean voltage of the electric arc decreases;

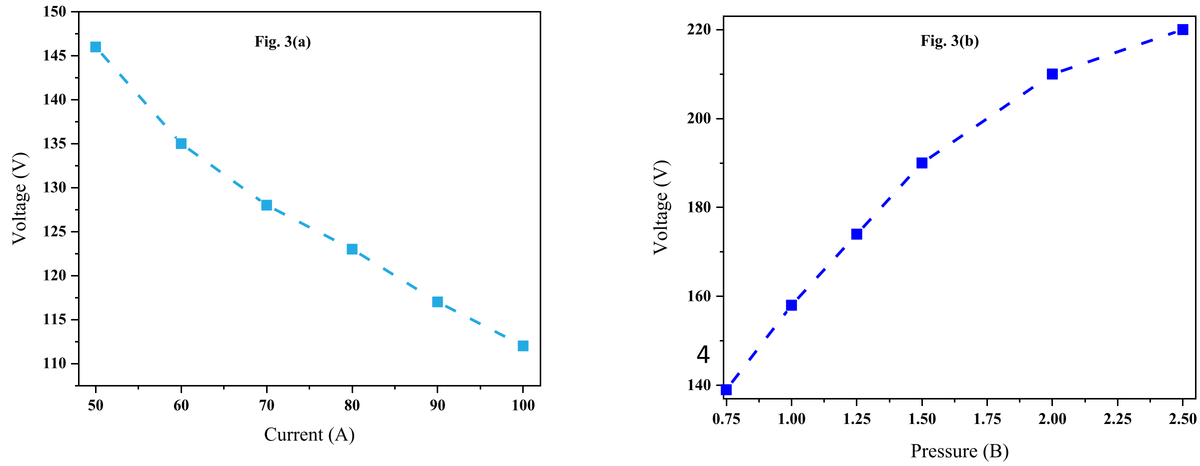

Figure 3. (a) Mean voltage versus current at a constant inlet gas pressure of 0.5 bar and (b) Mean voltage versus inlet gas pressure at a constant electric current of 100 A.

however, both the maximum and minimum voltage values show a slight decreasing trend. The arc exhibits a so-called 'restrike' behavior mode at all electric currents that are intensified upon increasing the current, as reported in table 1. The dominant voltage frequency diagram of the torch is depicted on the right side of figure 4 in red. It is derived from the FFT of the voltage-time diagram of the torch at the time interval of 0.02 s. With an increase in the electric current, the different available frequencies decrease, and a dominant frequency reaches its maximum value of 1350 Hz at a current of 100 A. The frequency of 300 Hz in the system is the fixed power supply frequency whose intensity remains almost constant. A three-phase power supply was used in these experiments. Each phase's difference is 120°, and the input power frequency is 50 Hz. Since the rectifier diode makes the current DC, the frequency value will always be 300 Hz due to a power supply.

On the left side of figure 5, a green graph is depicted in green, related to the voltage fluctuations of the plasma torch within the gas inlet pressure range of 0.75–2.5 bar at the current of 100 A. The sampling time of the plasma torch voltage is 0.02 s. Upon increasing the gas inlet pressure, the drag force on the electric arc column directs the arc toward the exit nozzle; consequently, the length of the electric arc and mean voltage of the torch increase. As observed, the amount of voltage fluctuation increases, i.e. the difference between the maximum and minimum voltage values. The 'restrike' behavior is attributed to the electric arc at all gas inlet pressures, yet its percentage is decreasing, as reported in table 1. The dominant voltage frequency diagram of the torch at different inlet pressures is depicted in pink color, which is derived from the FFT of the torch voltage-time diagram in the time interval of 0.02 s. Upon increasing the gas inlet pressure, the intensity of harmonics with different frequencies in the electric arc increases while the intensity of the dominant frequency of the electric arc decreases. As observed in the pink graphs, the harmonics have the same intensity at the current and gas inlet pressure of 100 A and 2.5 bar, respectively, in the voltage frequency range of 450 Hz – 9 kHz.

Post-operational visual inspection of the anode surface revealed different erosion patterns under varying experimental conditions. Under high current and low-pressure conditions (e.g. 100 A), the arc root remained relatively stable near the central axis, and the erosion pattern appeared concentrated and deeper, indicating a thin cold boundary layer and high local energy transfer. In contrast, at higher gas pressures (e.g. 2.5 bar), the increased gas velocity pushed the arc root to wander more across the anode surface, leading to a wider but more evenly distributed erosion zone, with reduced peak erosion depth. These findings are consistent with the interpretation that the cold boundary layer acts as an insulating buffer whose thickness modulates arc attachment behavior, energy deposition, and erosion geometry [28, 35].

Voltage fluctuations in the first case in different harmonics decrease, and only a few harmonics maintain their maximum intensity. As the electric current increases, so does the current density in the electric arc column, causing the plasma hot region to expand. As a result, the thickness of the cold boundary layer in the vicinity of the inner wall of the nozzle (anode) decreases, while voltage fluctuations in numerous measured harmonics increase. However, the number of harmonics decreases, implying that the number of electric arcs at various frequencies reduces as the energy density of electric arcs increases. In this regard, the energy transferred to the nozzle surface (anode) at the attachment point of the electric arc is more significant than that in other sections, hence more corrosion on the inner surface of the nozzle (anode) and power dissipation.

On the contrary, voltage fluctuations in the second case decrease, but the number of harmonics with less intensity in the voltage waveform increases. In this case, increasing the working gas inlet pressure increases the thickness of the cold boundary layer at the inner wall of the nozzle (anode),

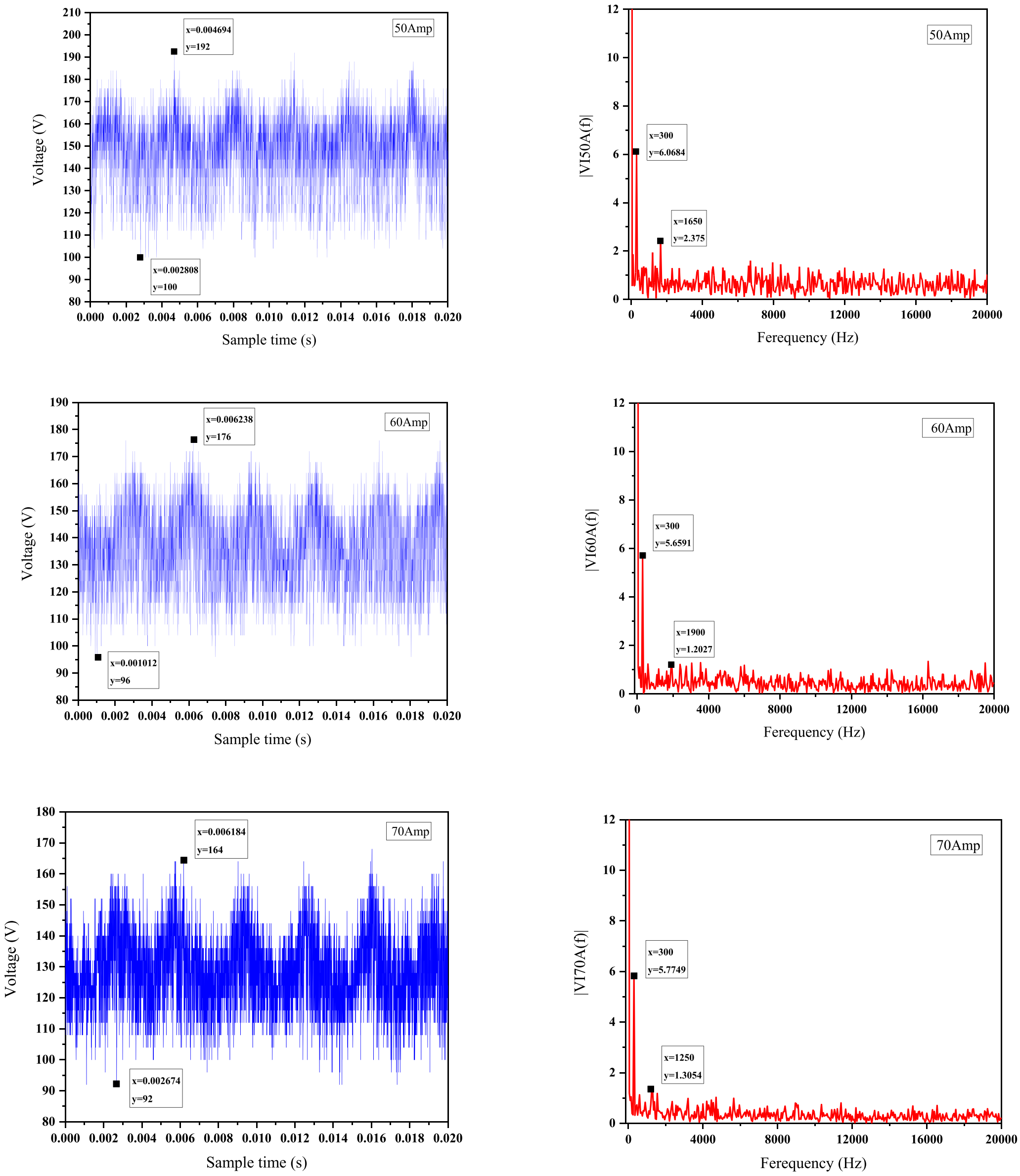

Figure 4. Voltage fluctuations of the torch in the current range of 50–100 A (left) and voltage frequencies of the torch in the current range of 50–100 A (right).

decreases voltage fluctuations in different harmonics, while increasing the number of harmonics. These findings confirm the formation of more electric arcs with a lower energy density, resulting in a decrease in the energy transferred to the nozzle (anode) at the electric arc attachment point, corrosion on the inner surface of the nozzle (anode), and power dissipation [28, 35, 36].

4.3. Investigation of the thermoelectric and thermodynamic characteristics

4.3.1. Torch thermal efficiency. Thermal efficiency is one of the significant parameters in plasma torch studies. Thermal efficiency in a DC plasma torch is obtained from the following equation:

$$\eta = \frac{E_{\text{input}} - Q_{\text{Cooling}}}{E_{\text{input}}}. \qquad (1)$$

The input power (E_{input}) in DC torches is obtained by multiplying the arc current by the arc voltage, and the energy loss is obtained as follows:

$$Q_{\text{Cooling}} = Q_{\text{rad}} + Q_{\text{conv}} + Q_{\text{CW}} \qquad (2)$$

where Q_{rad} is the amount of energy loss in the form of heat radiation from the nozzle surface, Q_{conv} the amount of energy loss in the form of convection from the contact surface between the nozzle and air, and Q_{CW} The amount of energy loss while cooling the electrodes with water. In this regard, the thermal efficiency of the DC plasma torch can be obtained as follows:

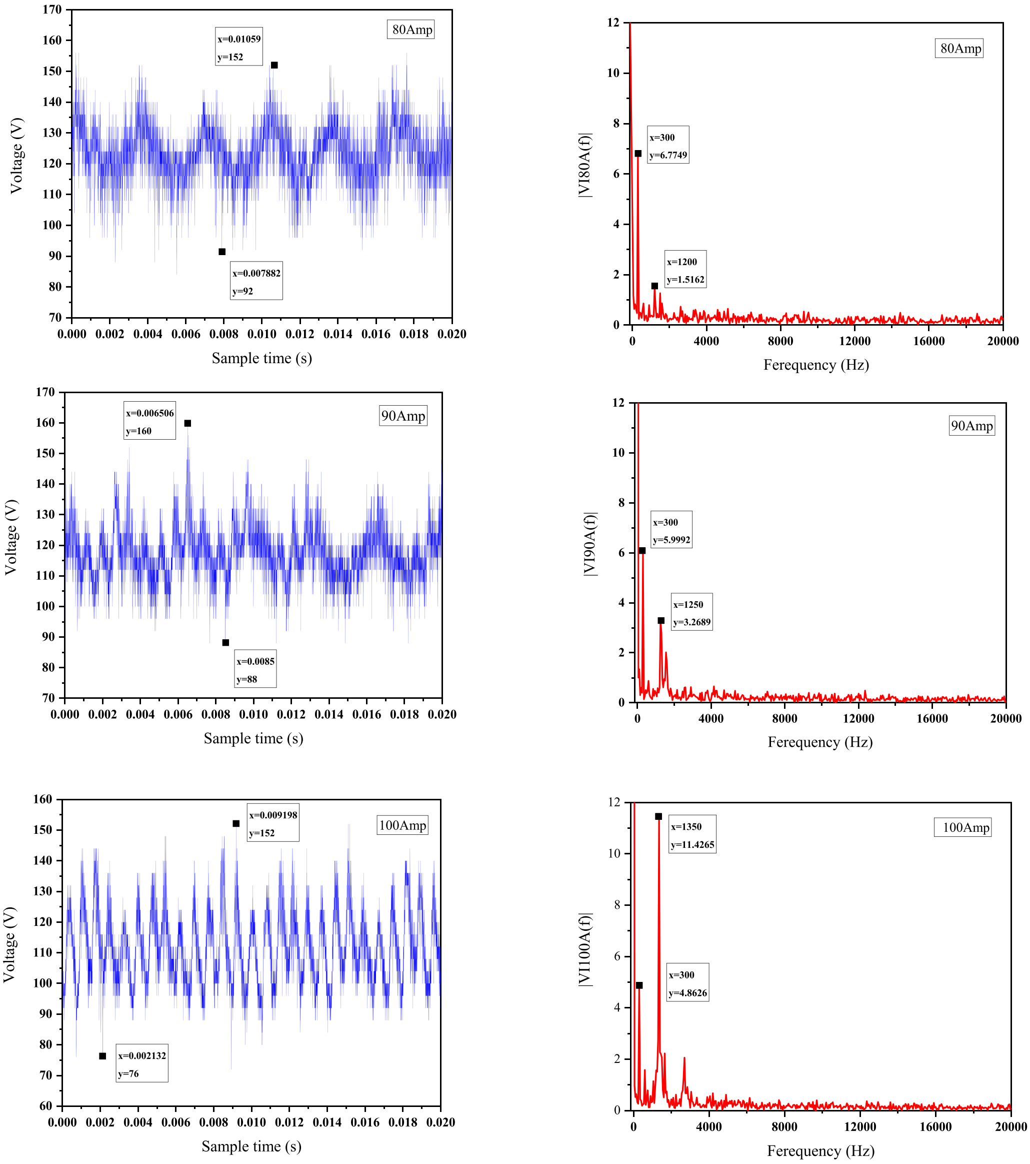

Figure 4. (Continued.)

$$\eta = \frac{I.V - \left(A\varepsilon\sigma\left(T_{\mathrm{s}}^4 - T_{\infty}^4\right) + Ah\left(T_{\mathrm{s}} - T_{\infty}\right) + 4.18c_{\mathrm{WC}}.q_{\mathrm{WC}}\left(T_2 - T_1\right)\right)}{I.V} \tag{3}$$

where η is the thermal efficiency, I the electric current of the torch, V is the electric voltage of the torch, A the torch outer surface that is in contact with the ambient air, ε the emissivity of the torch surface σ the Stefan-Boltzmann constant, h the convection heat transfer coefficient between the outer surface of the torch and the ambient air, c_{WC} the water specific heat, q_{WC} volume flux of torch cooling water, T_{s} the temperature of the outer surface of the torch, T_{∞} the temperature of the ambient air, and (T_2–T_1) the temperature difference between the inlet and outlet water in the torch [22]. Figure 6 shows the torch thermal efficiency variations as a function of the electric current and of the pressure.

Figure 6 shows that the thermal efficiency of the torch decreases upon increasing the electric current and increases when the gas inlet pressure increases. As observed in figure 6(a), at the constant working gas inlet pressure of 0.5 bar, with an increase in the electric current from 50 to 100 A, the thermal efficiency decreased from 80.5 to 75.1%.

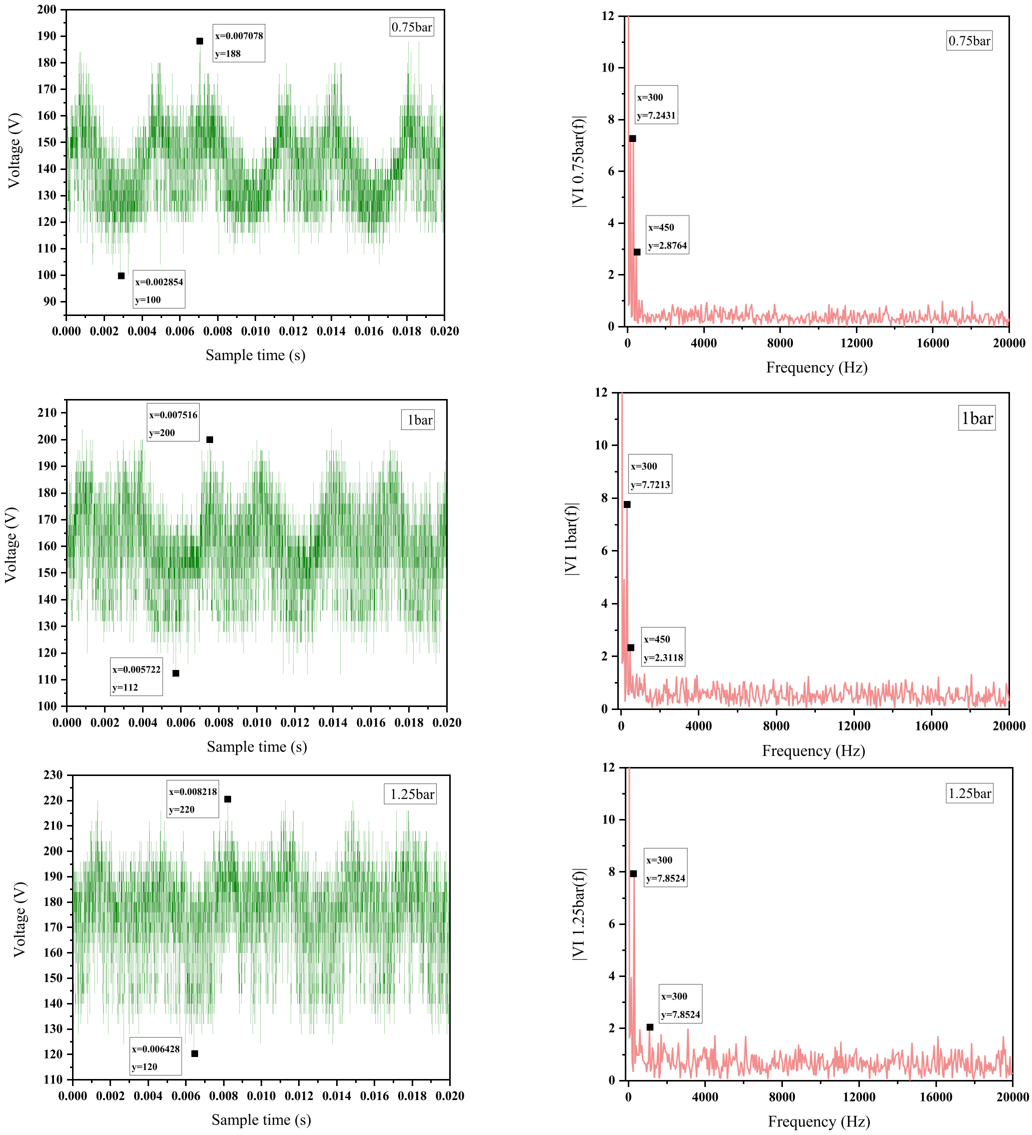

Figure 5. Voltage fluctuations (left) and voltage frequencies of the torch (right) at various nitrogen inlet pressures.

As shown in figure 6(b), the thermal efficiency of the torch increased from 80.5 to 87.2% at the constant electric current of 100 A with an increase in the working gas inlet pressure from 0.75 up to 2.5 bar.

Water-cooled electrodes provide the most to energy dissipation, while Q_{conv} and Q_{rad} contribute the least. In both cases, the amount of input power in the torch increased; that is, an increase in the gas inlet pressure and electric current increased the torch's input power. Figure 7(a) depicts the rise in the input power to the torch with an increase in the electric current, whereas figure 7(b) shows the increase in input power to the torch with an increase in the operating gas pressure. As clearly observed in figure 7, the slope of the constant pressure diagram is positive, indicating that the amount of power loss in the first case increases upon increasing the electric current at a constant gas pressure, hence a higher power loss rate. In the second case, however, the power loss decreases upon increasing the working gas pressure at a constant electric current, lowering the power loss rate. Based on this figure, it can be concluded that under a constant cooling condition, the power loss of the torch plasma in the case of an increase in the electric current is more than that of an increase in the working gas pressure.

4.4. Enthalpy characteristic of the torch versus the electric current and gas inlet pressure

Another important characteristic that should be considered in torches is enthalpy, i.e. the amount of energy transferred to the plasma. The value of the specific enthalpy of the output plasma in the torch is as follows:

$$h_{\mathrm{p}} = \frac{VI - (Q_{\mathrm{rad}} + Q_{\mathrm{conv}} + Q_{\mathrm{cw}})}{q_{\mathrm{wp}}} + h_0 \tag{4}$$

where h_{p} is the specific enthalpy of the plasma at the torch outlet, $I.V$ is the total electric power input to the torch (for DC torches), Q_{rad} is the total dissipated radiant power, Q_{conv}

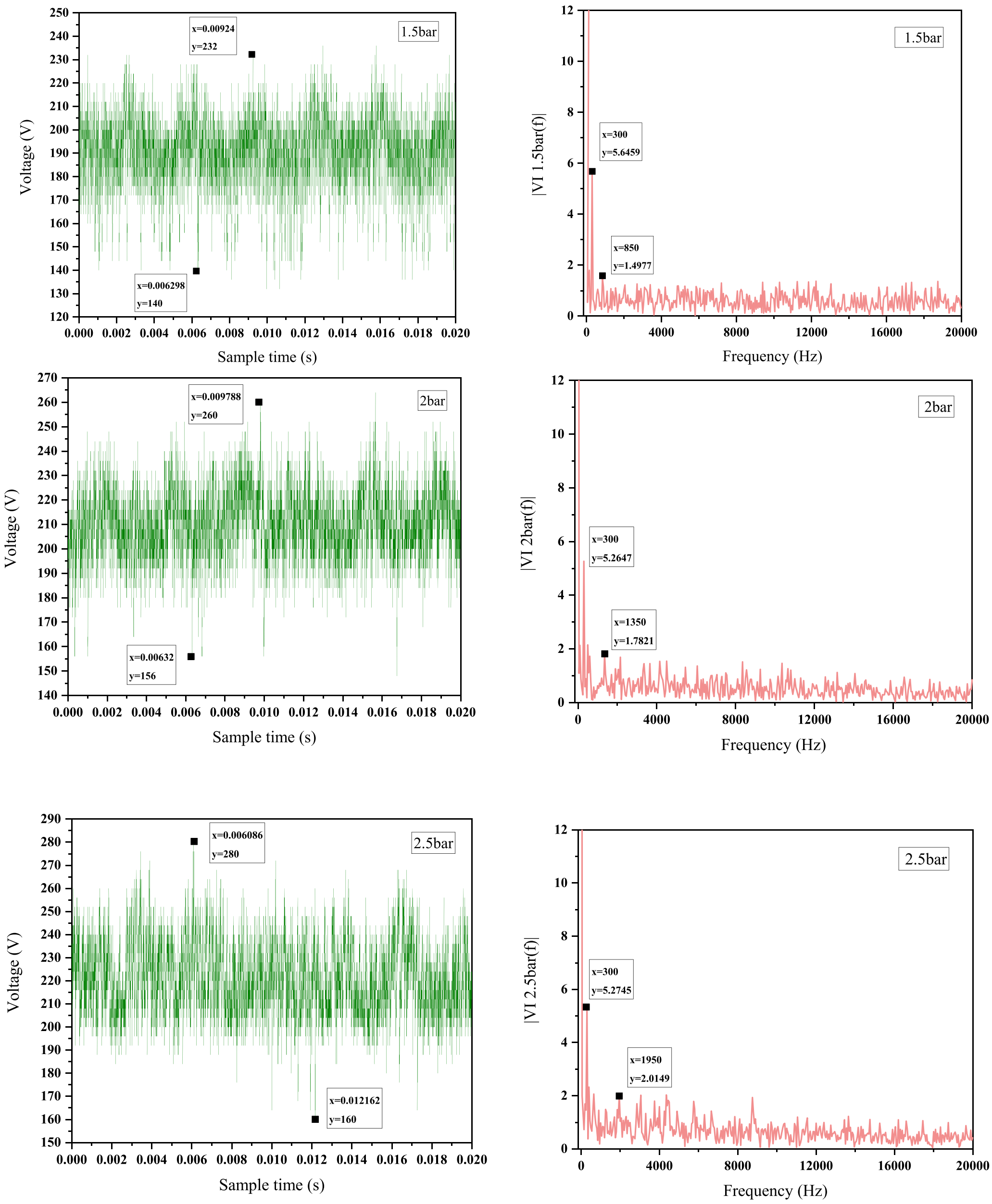

Figure 5. (Continued.)

Table 1. Comparison of the electric arc behavior in the nozzle for two conditions of constant gas inlet pressure and constant electric current.

Constant pressure of 0.5 bar			Constant current of 100 A			
Current (A)	Voltage fluctuation (%)	Torch voltage mode	Pressure (bar)	Flow rate (L min^{-1})	Voltage fluctuation (%)	Torch voltage mode
50	60	Restrike	0.75	9.2	68	Restrike
60	63	Restrike	1	12.5	65	Restrike
70	65	Restrike	1.25	13.3	61	Restrike
80	66	Restrike	1.5	15.7	58	Restrike
90	69	Restrike	2	17.8	55	Restrike
100	71	Restrike	2.5	19.2	52	Restrike

the total dissipated convective power between the torch and the surrounding air, Q_{cw} the total dissipated power due to water cooling, q_{wp} the mass flow rate of the torch working gas of (nitrogen), and h_0 the specific enthalpy of the torch working gas (nitrogen) before entering the torch which is equal 311.5 kJ kg^{-1} at the temperature of the test room. In

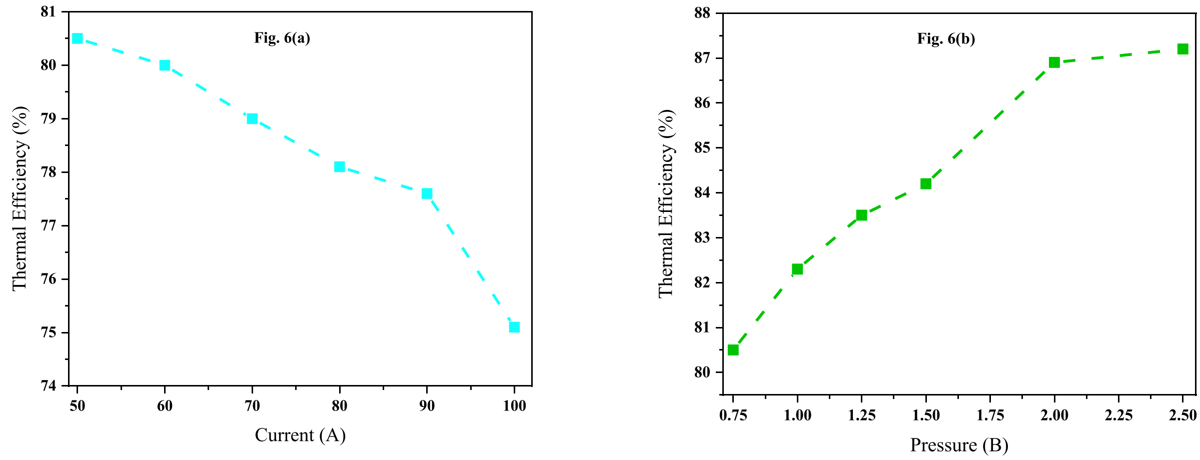

Figure 6. (a) Thermal efficiency versus current at a pressure of 0.5 bar and (b) thermal efficiency versus nitrogen inlet pressure at a current of 100 A.

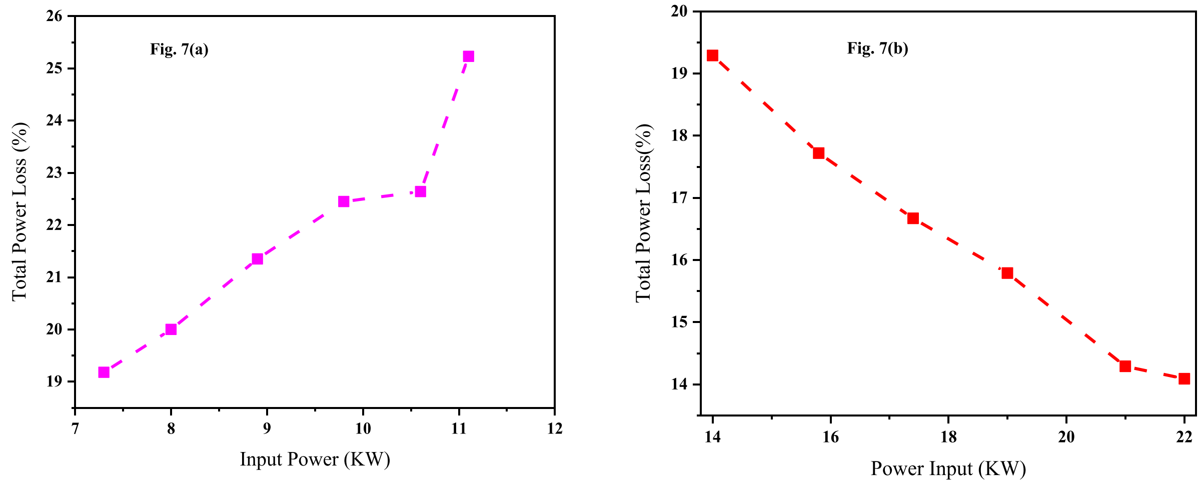

Figure 7. Total power loss versus input power under increasing currents and constant gas inlet pressure (a) and under raising the gas inlet pressure and constant current (b).

the above equation, the kinetic energy at the torch output is neglected due to the low speed of the output plasma [22]. Figure 8 depicts the specific enthalpy of the output plasma versus electric current and pressure of the inlet nitrogen gas.

According to figure 8, the specific enthalpy value of the plasma output from the torch increases with an increase in the electric current. At the same time, it decreases with an increase in the input gas pressure, leading to a rise in the mass flow rate of inlet nitrogen gas. Specifically, while there is an increase in the specific enthalpy in the first case, there is a decrease in this value in the second case. As observed in figure 8(a), with an increase in the electric current from 50 up to 100 A at the constant working gas pressure of 0.5 bar, the specific enthalpy of the plasma increased from 29.63 up to 44.41 MJ kg^{-1}. In addition, as shown in figure 8(b), with an increase in working gas pressure from 0.75 to 2.5 bar at the constant electric current of 100 A, the specific enthalpy of the plasma decreases from 34.69 to 8.85 MJ kg^{-1}.

4.5. Spectroscopic investigation of light emitted from the bulk plasma

4.5.1. Investigation of chemical and atomic species formed in the plasma. The atomic and molecular active species present in the plasma can be detected in this analysis. Given that these atoms and molecules are under quite a high temperature and exposed to an electric field, their energy is used for their internal energy (changes in electronic, vibrational, and rotational temperatures), excitation, and ionization. Once the radiation of the plasma flame is measured and analyzed, identification of the atomic and molecular species in the states of internal, excited, or ionized energy modes is made possible. In addition, applying various analytical techniques helps measure the species' electron, ion, excitation, and rotational or vibrational temperature. The characteristic of the thermodynamic equilibrium condition is the constant temperature in vibrational, rotational, electronic, and excitation modes [22, 29].

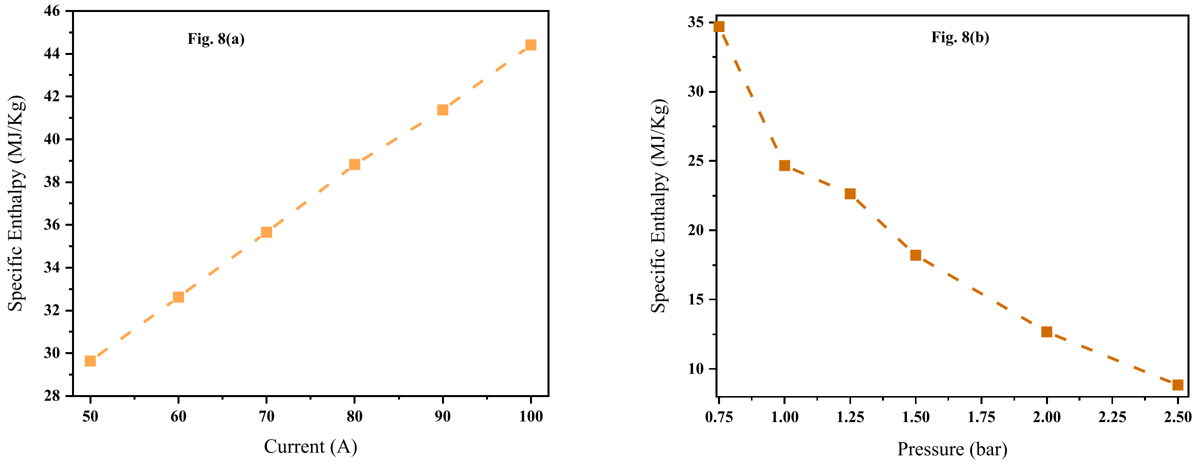

Figure 8. (a) Specific enthalpy of the output plasma versus current of the torch at gas inlet pressure of 0.5 bar and (b) specific enthalpy of the output plasma versus pressure of the inlet nitrogen gas of the torch at constant current of 100 A.

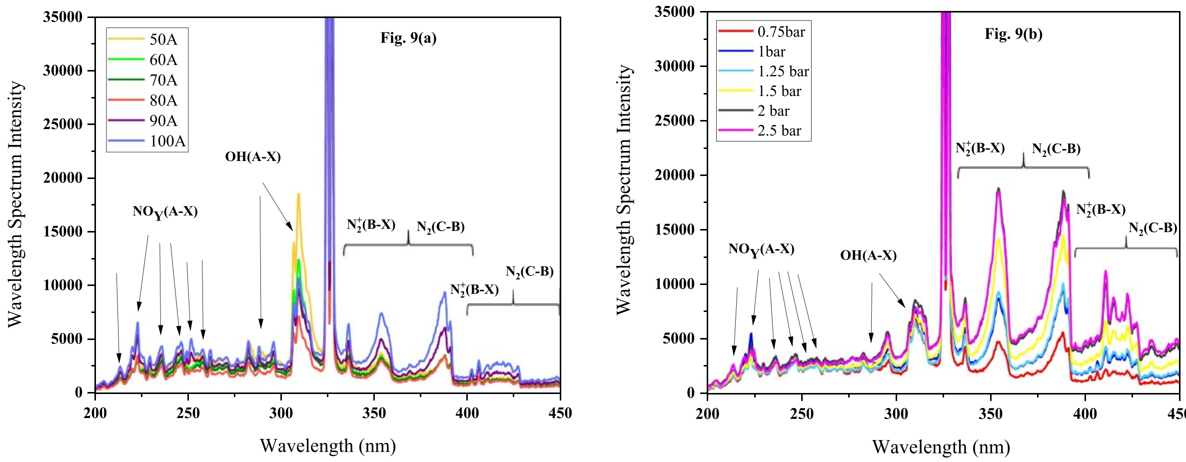

Figure 9. Nitrogen plasma spectroscopy in the air atmosphere in the wavelength range of 200–450 nanometers (a) at a constant pressure versus an increase in current and (b) at a constant current versus an increase in the inlet gas pressure.

Nitrogen plasma is formed in the ambient air at the atmospheric pressure during the experiment, hence the presence of OH, NO, N_2, O_2, N_2^+, O, N molecules in the plasma under study. Different peaks of molecules and atoms are formed at any temperature depending on the concentration of elements in the plasma gas. In addition, depending on the conditions, some species with the same wavelength range are found in molecules, while some species disappear in the radiation intensity of other species. It should be noted that in some cases, atomic peaks overlap with molecular ones. At high temperatures and low concentrations of water vapor in the plasma, the rotational and vibrational temperatures are determined by the molecular peaks NO_γ(A–X) and N_2^+(B–X), respectively [28]. At low temperatures below 5000 K or high concentrations of water vapor in the plasma, OH(A–X) branches R and P are used to determine the rotational temperature. It should be mentioned that the peaks of NO(A–X) and N_2 (C–B) dominate the OH peak at low concentrations of water vapor or very high temperatures, as a result of which, the OH peak disappears [36–38].

The analyses of nitrogen plasma in the wavelength range of 200–450 nm were separately carried out, and the existing molecular species were also identified. NO, and O_2 species overlap in the wavelength range of 200–270 nm depending on their intensity and temperature. Six peaks of NO_γ(A–X) molecule can be detected in figure 9; however, the intensity of NO peaks decreased due to the reduction in the oxygen percentage in the plasma region. The 270–320 nm wavelength range belongs to OH and N_2 molecules. At low temperatures up to 5000 K, the OH peak is almost the dominant one, while at temperatures higher than 5000 K, the OH peak disappears, and the N_2 peak becomes dominant. The wavelength ranges of 330–400 nm and 400–450 nm are attributed to N_2^+ and N_2 molecular species, respectively. The only detectable spectra here for N_2^+(0–0) and N_2^+(2–1) are at the wavelengths of 391.4 nm and 356.4 nm, respectively [29].

According to figure 9(a), with an increase in the electric current, the intensity of the peaks of N_2^+(B–X) and N_2(C–B) increases while that of the OH(A–X) peak decreases [28], which is indicative of an increase in the flame temperature.

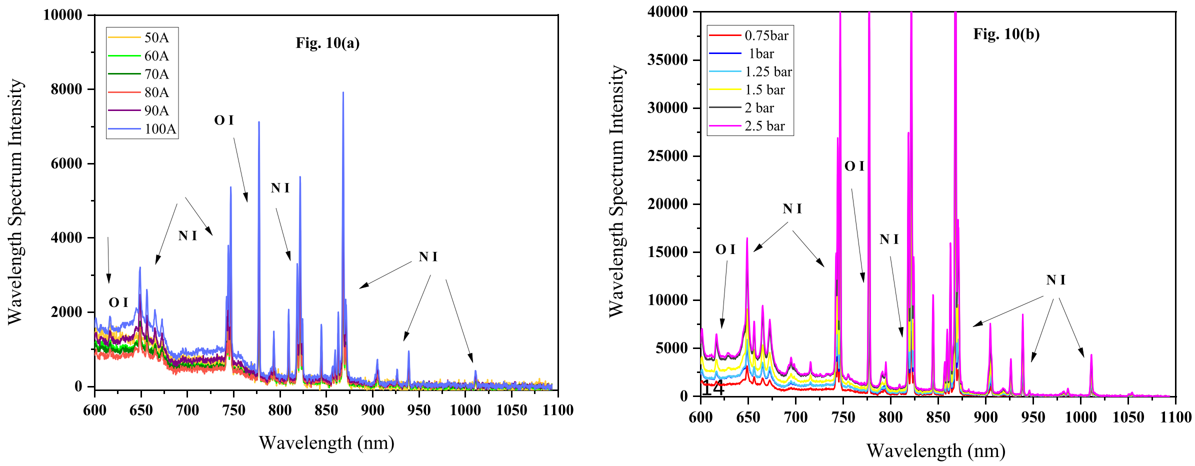

Figure 10. Spectroscopy of the nitrogen plasma in the air atmosphere in the wavelength range of 600–1100 nm (a) at a constant pressure versus an increase in current and (b) at a constant current versus an increase the gas inlet pressure.

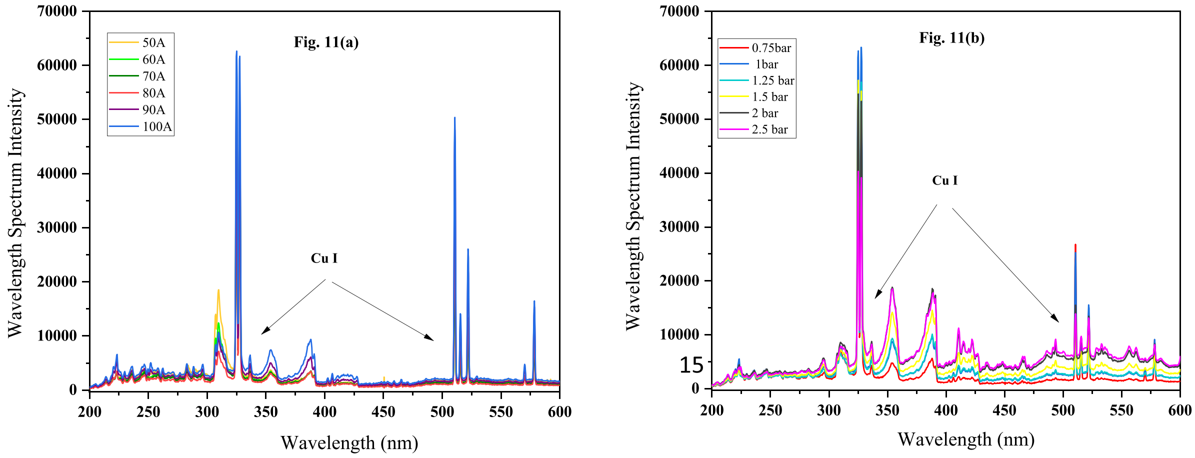

Figure 11. Spectroscopy of nitrogen plasma in the air atmosphere in the wavelength range of 200–600 nanometers (a) at a constant pressure versus an increase in the electric current and (b) at a constant electric current versus an increase in the inlet gas pressure.

In figure 9(b), with an increase in the inlet nitrogen flow rate, the concentration of N_2 molecules increases, and the intensity of the peaks of N_2^+(B–X) and N_2(C–B) increases. In general, it can be concluded that the molecular species of N_2^+(B–X) and N_2(C–B) increase in the first case mainly due to the rise in the plasma temperature, and the molecular species of N_2^+(B–X) and N_2(C–B) increase in the second case as a result of an increase in the number of nitrogen molecules that consequently decrease the temperature and enthalpy of the plasma.

Figure 10 demonstrates the spectroscopy of nitrogen plasma in the air atmosphere in the wavelength range of 600–1100, reporting the presence of nitrogen atoms (N I) and oxygen in the air atmosphere (O I). In figure 10(a), the intensity of nitrogen peaks increases with the electric current and temperature increase. In figure 10(b), with an increase in the nitrogen flow rate, the intensity of NI peaks considerably increases, indicating an increase in the nitrogen atoms in the plasma.

Another atom detected in the spectroscopy of the torch plasma output is Cu *I*. Due to the high temperature in the boundary layer between the copper electrode and plasma, copper melts and evaporates from the electrode surface. The presence of copper atoms as a suitable electrical and thermal conductor in plasma contributes to the plasma's thermal and electrical conductivity enhancement. The intensity of copper atom peaks can also measure electrode corrosion. As observed in figure 11(a), the peak wavelength of the Cu *I* atom increases upon increasing the electric current, hence an increase in the corrosion rate of the electrode. In figure 11(b), with an increase in the nitrogen flow rate, the peak intensity of the wavelength of the Cu *I* atom decreases, hence a decrease in the corrosion rate of the electrode. Figure 12 shows the intensity of copper atom peaks at 521.82, 515.32, and 510.55 nm of the radiation spectrum to clarify this issue better. The approximate corrosion rate of the nozzle (anode) can be defined as the changes in the intensity of the mentioned peaks at different electric currents and working gas pressures. In the first case, upon increasing the electric current from 50 to 100 A at a constant working gas inlet pressure of 0.5 bar, the intensity of the mentioned peaks increased, which is indicative of an increase in the number of copper atoms in the radiation spectrum of the plasma and correspondingly, a decrease in the thickness of the cold

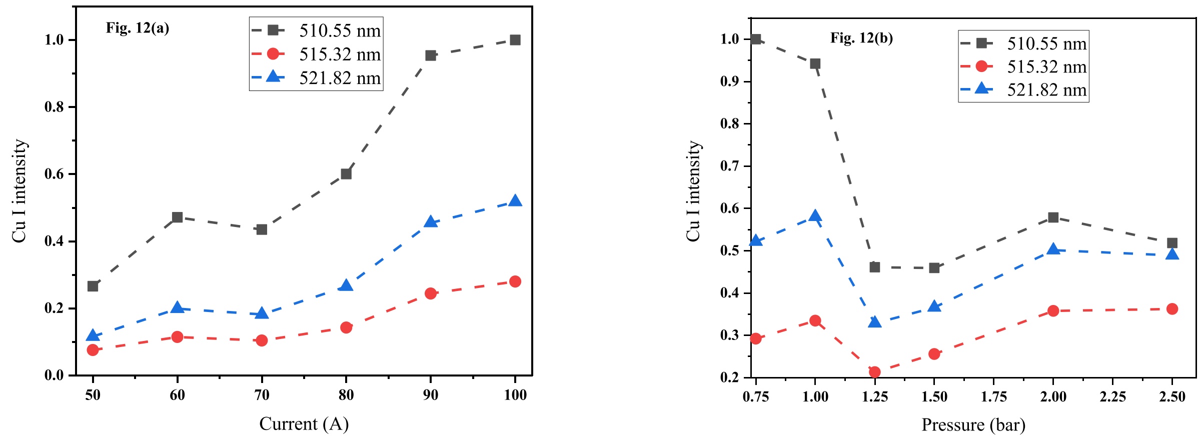

Figure 12. (a) and (b) Cu *I* intensity versus current at constant pressure (0.5 bar) and Cu *I* intensity versus pressure at constant current (100 A), respectively.

boundary layer around the inner wall of the nozzle (anode) and an increase in the corrosion rate in the mentioned area. In the second case, followed by increasing the pressure of the working gas from 0.75 up to 2.5 bar at the constant electric current of 100 A, the intensity of the mentioned peaks decreased, which indicates a decrease in the number of copper atoms in the radiation spectrum of the plasma and also an increase in the thickness of the cold boundary layer around the inner wall of the nozzle (anode), hence reduction of the corrosion rate in the inner wall of the nozzle (anode) [27]. A comparison was made between the first and second states according to the result of which the torch's two electric current and gas flow rate factors determine the temperature and rate of chemical species formed in the plasma. Any increase in the molecular and atomic peaks does not necessarily show a rise in the plasma temperature. Of note, an increase in the flow rate of the inlet gas can transform the plasma from a thermodynamic equilibrium state into a quasi-equilibrium state. Also, given the atomic peaks of copper Cu *I*, the amount of corrosion was found to have a direct relationship with the increase in the electric current and thermal efficiency, which follows an ascending trend.

To estimate the specific erosion rate of the anode, a quantitative calibration was performed at 100 A for 30 min of continuous torch operation. The mass of the copper nozzle before and after the test was measured using a precision balance with 0.1 mg resolution. A total mass loss of approximately 35 mg was observed, corresponding to an electric charge of 180 000 C. Thus, the specific erosion rate of the copper anode was estimated to be 0.000 194 mg C^{-1} or 0.7 mg per Ah. This value, although approximate, is consistent with the increase in Cu *I* peak intensities shown in figure 12(a) and confirms the correlation between electric current density, thermal stress, and anodic erosion. This estimation provides a useful reference for predicting the electrode lifetime and maintenance scheduling.

4.6. Analysis of the excitation and rotational temperature of atoms and molecules formed in the plasma

One of the appropriate methods for determining the excitation temperature of atoms is to draw the Boltzmann plot that shows the slope of the excitation temperature diagram. This method is one of thermometry's most widely used techniques since it does not need a standard light source for calibration [39]:

$$\ln\left(\frac{I_{\mathrm{ki}}\lambda_{\mathrm{ki}}}{g_{\mathrm{k}}A_{\mathrm{ki}}}\right) = \ln K - \frac{E_{\mathrm{k}}}{k_{\mathrm{B}}T_{\mathrm{ext}}}. \quad (5)$$

I_{ki} stands for the spectral line intensity, λ_{ki} the excited atom wavelength, g_{k} the statistical weight of the upper atomic state, A_{ki} the transition probability, E_{ki} the energy difference between the two excitation levels, and k_{B} Boltzmann constant. One method that confirms the thermodynamic equilibrium is to draw a diagram where the excitation, rotational, and vibrational temperatures converge into a constant temperature [22]. The characteristics of the excitation of transitions and intensities obtained from the spectroscopy given in figure 10 were considered to draw the Boltzmann plot for different states, and the value of the nitrogen atom excitation temperature was obtained from the slope of the diagrams. Table 2 shows the excitation temperature of the nitrogen atom for the first and second conditions. In both cases, there was an increase in the excitation temperature of the nitrogen atom, but it is not the main reason for the increase in the flame's temperature exiting the torch. Molecular temperature and peaks were also investigated to determine the flame temperature. On the left column of this table is shown the excitation temperature of the nitrogen atom versus the increase in the electric current at a constant pressure of 0.5 bar, while on the right column is the excitation temperature of the nitrogen atom versus the increase in the input working gas pressure at the electric current of 100 A.

In thermal, quasi-thermal, and non-thermal plasmas, the closest temperature to the gas temperature that can be considered as the mean temperature of the flame exiting the torch is defined as the rotational temperature of the molecular species in the plasma. In this regard, NO–OH spectroscopy is used in air plasmas or air atmospheres at temperatures below 5000 K [29]. Notably, the OH peaks disappear at temperatures higher than 5000 K due to overlapping N_2(C–B) peaks with OH peaks. However, according to the spectroscopic chart in the wavelength range of 200–450 nm in figure 9, the OH

Table 2. Excitation temperature of the nitrogen atom.

Constant pressure of 0.5 bar		Constant current of 100 A	
Current (A)	N I Excitation temperature (K)	Pressure (bar)	N I Excitation temperature (K)
50	2602	0.75	2830
60	2614	1	2975
70	2620	1.25	3081
80	2624	1.5	3138
90	2646	2	3192
100	2683	2.5	3226

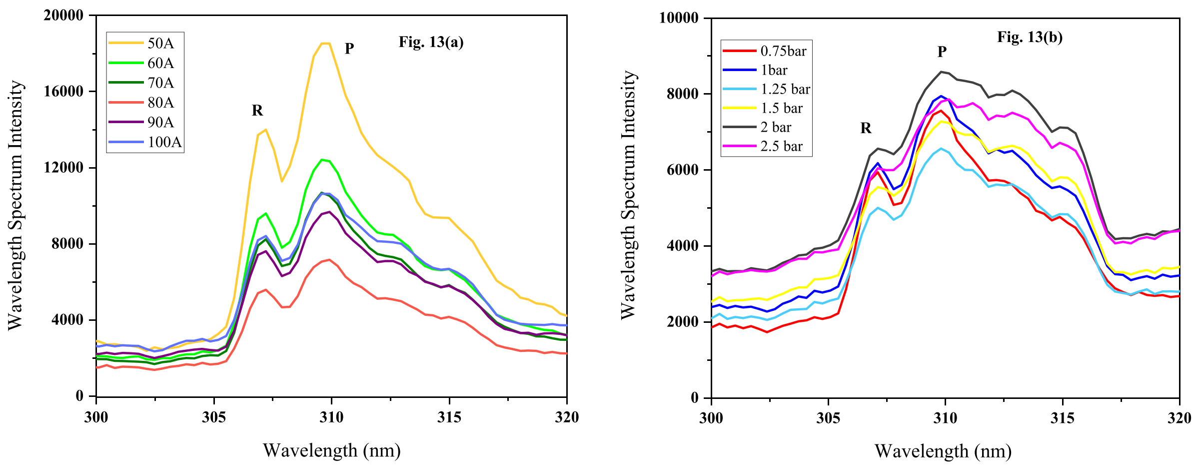

Figure 13. Spectroscopy of nitrogen plasma in the air atmosphere in the wavelength range of 300–320 nanometers (a) at a constant pressure versus an increase in current and (b) at a constant current versus an increase in the inlet gas pressure.

peaks overlap with N_2(C–B) ones, indicating that the temperature of the output flame of the torch is less than 5000 K. The P and R branches of the OH(0–0) transition was considered to obtain the rotational temperature of the OH molecule. The intensity ratio of the spectrum of the *P* branch to the *R* branch is always a coefficient of the rotational temperature of the OH molecule [29]. Figure 13 shows the obtained spectrum in the 300–320 nm range, confirming the presence of *P* and *R* branches of the OH (0–0) transition.

The OH spectrum is formed due to H_2O water vapor in the atmosphere. For this reason, the rotational temperature of the OH molecule can be considered as the temperature of the plasma flame. Table 3 comparatively reports the rotational temperature of the OH molecule. The column on the left shows the rotational temperature of the OH molecule versus an increase in the electric current at the constant pressure of 0.5 bar, and the column on the right shows the rotational temperature of the OH molecule versus an increase in the pressure of the input working gas in the electric current of 100 A. While the rotational temperature of the OH molecule increase in the first case, it decreases in the second case. This observation is more consistent with the output plasma enthalpy diagram results. A comparison was made between tables 2 and 3 according to the results of which the increase in the rotational temperature of the OH molecule is consistent with the increase in the excitation temperature of the nitrogen atom in the first case; however, in the second case, no such consistency can be found. These comparisons show that the plasma is not in thermodynamic equilibrium but is in a quasi-equilibrium state. In this case, the rotational temperature of the OH molecule can be considered as the flame's temperature exiting the torch.

The rotational temperature of OH molecules was estimated using the spectral intensities of the P and R branches of the OH(A–X) transition in the range of 306–312 nm. The fitting process followed standard Boltzmann methods, and the spectral resolution was 0.5 nm. The overall uncertainty in the determined rotational temperature is estimated to be approximately ±200 K, based on the resolution, fitting accuracy, and signal-to-noise ratio. This uncertainty agrees with prior studies using OH spectroscopy for thermal plasma characterization under similar conditions [29, 36].

It should be noted that the spectroscopic measurements were obtained using a fixed fiber-optic probe positioned 1 cm downstream from the nozzle exit and 10 cm radially from the plasma jet, aligned with the center of the flame. The field of view corresponds to the central line-of-sight of the jet. Consequently, the reported temperatures are based on axial measurements only, without spatial resolution across the jet section. While this provides a good indication of the plasma core conditions, future work will aim to include radial scanning for a more complete characterization.

Table 3. The rotational temperature of the OH molecule in the formed plasma.

Constant pressure of 0.5 bar		Constant current of 100 A	
Current (A)	OH rotational temperature (K)	Pressure (bar)	OH rotational temperature (K)
50	3159	0.75	3391
60	3295	1	3343
70	3391	1.25	3295
80	3441	1.5	3249
90	3465	2	3222
100	3492	2.5	3204

5. Conclusion

This study investigated a novel, developed, and produced DC non-transferred plasma torch for pyrolysis of liquid carbon-based materials using nitrogen as a working gas. Plasma diagnostic techniques are used to characterize (electrically, thermodynamically, and chemically) this innovative torch in which feed waste/material is injected 20 mm from the nozzle exit. The experiments were carried out under two conditions: (a) increasing electrical current while keeping nitrogen gas input pressure, and (b) constant electrical current and rising nitrogen gas inlet pressure. As the data reveal, with constant injected nitrogen gas pressure, a rise in electric current, which may be interpreted as an increase in electron density in the plasma arc column, causes a voltage decrease. However, while the electric current remains constant, increasing the pressure of the injected nitrogen gas reverses the tendency. The maximum 220 V and the minimum of 112 V were recorded for 100 A, and nitrogen inlet pressure was 2.5 and 0.5 bar, respectively. Moving electric arcs showed a restrike mode at all electrical current values and injected gas pressures in both situations. The torch's thermal efficiency ranges from 80.5 to 75.1% and 80.5 to 87.2% under test conditions, increasing the electric current and injected gas pressure, respectively. Given the amount of power loss, the user is free to optimize the torch to the required conditions. The obtained enthalpy of 44.41 MJ kg^{-1}, with an electric current of 100 A, injected gas pressure of 0.5 bar, and thermal efficiency of 75.1%, makes it an ideal environment for pyrolysis. The flame temperature of approximately 3500 K, which is higher than the other conditions, validates this consideration. Our electrical and spectroscopic characterizations established that the system maintains stable discharge and energy delivery, both of which are vital for continuous processing of viscous carbon-rich liquids.

Data availability statement

All data that support the findings of this study are included within the article (and any supplementary files).

Author contributions

Parham Firoozi
Investigation (equal), Writing – original draft (equal)

Mohammad Reza Khani 0000-0001-7753-1780
Conceptualization (lead), Resources (equal), Supervision (equal), Validation (equal)

Farzaneh Ostovarpour
Methodology (equal), Resources (equal), Visualization (equal)

Babak Shokri 0000-0002-8242-5111
Supervision (equal), Validation (equal)

Abel Rouboa
Formal analysis (equal), Writing – review & editing (equal)

Eliseu Monteiro 0000-0002-3904-337X
Formal analysis (equal), Writing – review & editing (equal)

References

[1] Samal S 2017 Thermal plasma technology: the prospective future in material processing *J. Clean. Prod.* **142** 3131–50
[2] Mostaghimi J and Boulos M I 2015 Thermal plasma sources: how well are they adopted to process needs? *Plasma Chem. Plasma Process.* **35** 421–36
[3] Fauchais P 2004 Understanding plasma spraying *J. Phys. D* **37** R86
[4] Fauchais P, Vardelle M and Goutier S 2016 Latest researches advances of plasma spraying: from splat to coating formation *J. Therm. Spray Technol.* **25** 1534–53
[5] Vardelle A, Moreau C, Themelis N J and Chazelas C 2015 A perspective on plasma spray technology *Plasma Chem. Plasma Process.* **35** 491–509
[6] Shigeta M and Murphy A B 2011 Thermal plasmas for nanofabrication *J. Phys. D: Appl. Phys.* **44** 174025
[7] Baskoro A S and Supriadi S 2019 Review on plasma atomizer technology for metal powder in *MATEC Web of Conf.* Vol 269 p 5004
[8] Murphy A B 2015 A perspective on arc welding research: the importance of the arc, unresolved questions and future directions *Plasma Chem. Plasma Process.* **35** 471–89
[9] Safa S and Soucy G 2014 Liquid and solution treatment by thermal plasma: a review *Int. J. Environ. Sci. Technol.* **11** 1165–88
[10] Karimi H, Khani M R, Gharibi M, Mahdikia H and Shokri B 2020 Plasma pyrolysis feasibility study of spent petrochemical catalyst wastes to hydrogen production *J. Mater. Cycles Waste Manage.* **22** 2059–70
[11] Pitrez P, Monteiro E and Rouboa A 2025 Energy recovery from infectious hospital waste and its safe neutralization *Int. J. Hydrog. Energy* **105** 1103–13
[12] Prado E S P, Miranda F S, de Araujo L G, Petraconi G and Baldan M R 2020 Thermal plasma technology for

radioactive waste treatment: a review *J. Radioanal. Nucl. Chem.* **325** 331–42
[13] Fasihi M, Mohammadhosseini B, Ostovarpour F, Abbassi Shanbehbazari M S, Khani M R and Shokri B 2022 (Digital presentation) potential application of plasma pyrolysis in dairy industries *ECS Meeting Abstracts* vol 242 p 2618
[14] Okati A, Khani M R, Shokri B, Monteiro E and Rouboa A 2021 Numerical modeling of plasma gasification process of polychlorinated biphenyl wastes *Energy Rep.* **7** 270–85
[15] Tendero C, Tixier C, Tristant P, Desmaison J and Leprince P 2006 Atmospheric pressure plasmas: a review *Spectrochim. Acta B* **61** 2–30
[16] Venkatramani N 2002 Industrial plasma torches and applications *Curr. Sci.* **83** 254–62 (available at: www.jstor.org/stable/24106883)
[17] Zhukov M F and Zasypkin I M 2007 *Thermal Plasma Torches: Design, Characteristics, Application* (Cambridge Int Science Publishing)
[18] Boulos M I, Fauchais P L and Pfender E 2019 *Handbook of Thermal Plasmas* (Springer)
[19] Rajabian M, Gravelle D V and Vacquié S 2004 Measurements of temperature and electron number density in a dc argon–nitrogen plasma torch—supersonic operation *Plasma Chem. Plasma Process.* **24** 285–305
[20] Kim S-W, Park H-S and Kim H-J 2003 100 kW steam plasma process for treatment of PCBs (polychlorinated biphenyls) waste *Vacuum* **70** 59–66
[21] Nishikawa H, Ibe M, Tanaka M, Takemoto T and Ushio M 2006 Effect of DC steam plasma on gasifying carbonized waste *Vacuum* **80** 1311–5
[22] Ni G, Zhao P, Cheng C, Song Y, Toyoda H and Meng Y 2012 Characterization of a steam plasma jet at atmospheric pressure *Plasma Sources Sci. Technol.* **21** 15009
[23] Cao X, Yu D, Xiao M, Miao J, Xiang Y and Yao J 2016 Design and characteristics of a laminar plasma torch for materials processing *Plasma Chem. Plasma Process.* **36** 693–710
[24] Obraztsov N V, Safronov A A, Subbotin D I, Ivanov D and Dudnik J D 2019 The usage of low-voltage AC plasma torch for polystyrene gasification *IOP Conf. Ser: Mater. Sci. Eng.* **643** 12076
[25] Chau S W, Lu S Y and Wang P J 2021 Study on arc and flow characteristics of a non-transferred DC steam torch *J. Chin. Inst. Eng.* **44** 646–58
[26] Tamošiūnas A, Valatkevičius P, Grigaitiene V and Valinčius V 2012 Water vapor plasma torch: design, characteristics and applications *Int. J. Phys. Math. Sci.* **6** 1444–7
[27] Chau S W, Hsu K L, Lin D L and Tzeng C C 2007 Experimental study on copper cathode erosion rate and rotational velocity of magnetically driven arcs in a well-type cathode non-transferred plasma torch operating in air *J. Phys. D: Appl. Phys.* **40** 1944
[28] Nogues E, Fauchais P, Vardelle M and Granger P 2007 Relation between the arc-root fluctuations, the cold boundary layer thickness and the particle thermal treatment *J. Therm. Spray Technol.* **16** 919–26
[29] Laux C O, Spence T G, Kruger C H and Zare R N 2003 Optical diagnostics of atmospheric pressure air plasmas *Plasma Sources Sci. Technol.* **12** 125
[30] Kubota Y, Hara T, Ichiki R, Yamaguchi N and Takemura Y 2009 Spectroscopic analysis of nitrogen atmospheric plasma jet *J. Plasma Fusion Res.* **8** 740–3
[31] Fauchais P and Vardelle A 1997 Thermal plasmas *IEEE Trans. Plasma Sci.* **25** 1258–80
[32] Solonenko O 2003 Electric arc generators of thermal plasma: review *Thermal Plasma Torches and Technologies: Plasma Torches: Basic Studies and Design* vol 1 (Cambridge International Science Publishing) pp 1–19
[33] Mogensen P and Thörnblom J 1987 Electrical and mechanical technology of plasma generation and control *Plasma Technology in Metallurgical Processing* (Iron and Steel Society, Inc) pp 65–76
[34] Yas' Ko O I 1969 Correlation of the characteristics of electric arcs *J. Phys. D: Appl. Phys.* **2** 733
[35] Duan Z and Heberlein J 2002 Arc instabilities in a plasma spray torch *J. Therm. Spray Technol.* **11** 44–51
[36] Foltin V, Leštinská L and Machala Z 2006 Spectroscopic investigations of atmospheric pressure microwave torch nitrogen plasma jet *Czech. J. Phys.* **56** B712–20
[37] Chen C-J and Li S-Z 2015 Spectroscopic measurement of plasma gas temperature of the atmospheric-pressure microwave induced nitrogen plasma torch *Plasma Sources Sci. Technol.* **24** 35017
[38] Kawahara N, Hashimoto S and Tomita E 2017 Spark discharge ignition process in a spark-ignition engine using a time series of spectra measurements *Proc. Combust. Inst.* **36** 3451–8
[39] Lakomsky V I 2000 *Oxide Cathodes for the Electric Arc* (*Welding and Surfacing Reviews Series* vol 13) (Netherlands Routledge) pp 1–121